Check for updates

A reactive electrochemical filter system with an excellent penetration flux porous Ti/SnO₂–Sb filter for efficient contaminant removal from water†

Kui Yang,[ab] Hui Lin, (ID) *[b] Shangtao Liang,[c] Ruzhen Xie,[d] Sihao Lv,[b] Junfeng Niu,[b] Jie Chen[b] and Yongyou Hu (ID) *[ae]

Tubular porous Ti/SnO₂–Sb filters with excellent penetration flux (~61.94 $m^3\ m^{-2}\ h^{-1}\ bar^{-1}$) and electrochemical activity were prepared by a sol–gel method using low-cost porous titanium filters as the substrates. The porous Ti/SnO₂–Sb filters were used as anodic reactive electrochemical membranes to develop reactive electrochemical filter systems, by combining membrane filtration technology with the electrooxidation process, for water treatment. A convection-enhanced rate constant of $4.35 \times 10^{-4}\ m\ s^{-1}$ was achieved for $Fe(CN)_6^{4-}$ oxidation, which approached the kinetic limit and is the highest reported in an electrochemical system. The electrooxidative performance of the reactive electrochemical filter system was evaluated with 50 mg L^{-1} rhodamine B (RhB). The results showed that the reactive electrochemical filter system in flow-through mode resulted in an 8.6-fold enhancement in RhB oxidation as compared to those in flow-by mode under the same experimental conditions. A normalized rate constant of $5.76 \times 10^{-4}\ m\ s^{-1}$ for RhB oxidation was observed at an anode potential of 3.04 V vs. SCE, which is much higher than that observed in a reactive electrochemical filter system with carbon nanotubes and/or Ti₄O₇ (1.7×10^{-5}–$1.4 \times 10^{-4}\ m\ s^{-1}$). The electrical energy per order degradation (EE/O) for RhB was as low as 0.28 kW h m^{-3} in flow-through mode, with a relatively short residence time of 9.8 min. The overall mineralization current efficiency (MCE) was calculated to be 83.6% with ~99% RhB removal and ~51% TOC removal. These results illustrate that this reactive electrochemical filter system is expected to be a promising method for water treatment.

1. Introduction

The electrooxidation process has emerged as a promising technique for the destruction of various toxic refractory organic pollutants in aqueous solutions due to its mild reaction conditions, strong oxidation ability, easy operation and environmental compatibility.[1] Recently, it has been successfully applied in treating industrial wastewater including paper production wastewater,[2] textile wastewater,[3–5] landfill leachate[6,7] and refractory perfluorinated compounds.[8,9]

However, the relatively long retention time and low current efficiency limit its large-scale application. This is because electrooxidation reactions are specific to heterogeneous catalysis, and the mass transfer rate of the traditional electrooxidation process limits the overall efficiency of the reaction system.[10] Traditional electrooxidation reactors typically use parallel plate electrodes, in which wastewater is pumped through the narrow flow channel (in the range of mm to cm) between the anode and cathode either in one-pass or recirculation mode. This is defined as flow-by mode. In this fluid dynamic state, a thin stagnant boundary layer is formed near the surface of the electrode. In addition, hydroxyl radicals (˙OH) formed via the oxidation of water on the anode surface can react unselectively with a wide range of organics at an extremely high reaction rate (~10^{10} L $mol^{-1}\ s^{-1}$).[11,12] Experimental studies and modeling data suggest that the reaction between organics and ˙OH only occurs in a narrow zone, within 1 μm around the anode surface.[11,12] However the boundary layer of the electrode surface is thicker than 100 μm in typical flow-by modes,[10] which is much thicker than the

aSchool of Environment and Energy, South China University of Technology, Guangzhou 510006, P. R. China. E-mail: 201520132411@mail.scut.edu.cn; ppyyhu@scut.edu.cn; Fax: +86-20-3938-0508; Tel: +86-136-0274-6125

bSchool of Environment and Civil Engineering, Dongguan University of Technology, Dongguan 523808, P. R. China. E-mail: linhui@bnu.edu.cn; 23817001@qq.com; junfengn@bnu.edu.cn; 1875898657@qq.com; Fax: +86-769-3901-8706; Tel: +86-769-3901-8706

cAECOM Inc., Environment, Atlanta, Georgia 30309, USA. E-mail: sliang@uga.edu

dCollege of Architecture and Environment, Sichuan University, Chengdu 610065, P. R. China. E-mail: xieruzhen@scu.edu.cn

eThe Key Lab of Pollution Control and Ecosystem Restoration in Industry Clusters, Ministry of Education, South China University of Technology, Guangzhou Higher Education Mega Centre, Guangzhou, 510006, PR China

† Electronic supplementary information (ESI) available. See DOI: 10.1039/c8ra00603b

thickness of the reaction zone between organics and ˙OH. Under this circumstance, the diffusion of organics to the reaction zone is extremely difficult, resulting in a low normalized mass transfer rate constant of 10^{-6} to 10^{-5} m s^{-1}.[10,13,14] Therefore the reaction rate is limited by the mass transfer rate, which lowers the overall current efficiency.

In order to overcome the mass transfer limitation in the traditional electrooxidation process, researchers have utilized $Ti_nO_{2(n-1)}$ (n = 4 to 6) conductive ultrafiltration ceramic membranes[13,15–17] or carbon nanotube (CNT) networks[14,18–20] as anodes to build anodic reactive electrochemical filter systems, by combining membrane filtration technology with the electrooxidation process, in flow-through mode for water treatment. The thickness of the boundary layer is a function of the cross-flow velocity and/or the turbulence of the flow. In flow-through mode, water moves adjectively through the pores on the electrode materials. This process minimizes the thickness of the boundary layer, thus greatly improving the mass transfer rate of pollutants moving towards the anode surface zone. However, $Ti_nO_{2(n-1)}$ conductive ceramic ultrafiltration membranes with nanopores may be easily contaminated because industrial effluents tend to be of poor water quality and adding a pre-treatment increases the total cost. CNTs are not active for ˙OH production, and their high cost further limits the large-scale application of CNT networks. Consequently, it's urgent to seek inexpensive, porous electrode materials with macropores with excellent permeability for water treatment. Recently, Li et al.[21] prepared a porous Ti/SnO$_2$–Sb anode in flow-through mode from porous titanium tubes with an average pore size of 2.5 μm to degrade pyridine. Compared to the traditional flow-by mode, the flow-through mode increased the pyridine degradation rate by 43.9%. However, the mass transfer efficiency of this electrochemical system was not mentioned.

As typical "non-active" electrodes, Sb-doped SnO$_2$ anodes have many advantages such as cost-effectiveness, being easy to prepare, high oxygen evolution potential and good catalytic activity.[21–24] Thus, in this study, we focus on understanding the mechanism of electrooxidation by studying the mass transfer rate of a flow-through system using tubular Ti/SnO$_2$–Sb filters, with an average pore size of about 30 μm, as reactive electrochemical membranes. The standard probing molecule $Fe(CN)_6^{4-}$ was used to assess the mass transfer performance of the reactive electrochemical filter system for direct oxidation (outer-sphere charge transfer). Rhodamine B (RhB, the molecular structure is shown below) was chosen as a model refractory organic pollutant because RhB is a common dye in the triphenylmethane family and has been used extensively in the textile, printing, food and cosmetic industries.[25,26] The effects of the operating mode and the applied anode potential on the performance of the reactive electrochemical filter system were investigated. To further verify the feasibility of the reactive electrochemical filter system for water treatment, mineralization current efficiency and energy consumption were also assessed.

$C_{28}H_{31}ClN_2O_3$

479.2 g mol^{-1}

Rhodamine B
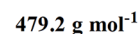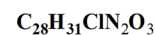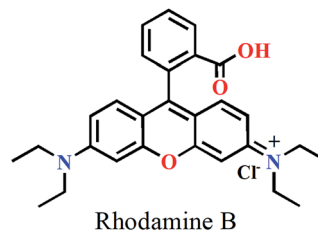
2. Experimental

2.1. Materials

Commercially available sintered powder porous tubular titanium filters (Baoji Yinggao Metal Material Co., Ltd. China) with inner and outer diameters of 26 and 30 mm, respectively, and a length of 100 mm were used as substrates. Sodium hydroxide (NaOH), oxalic acid ($C_2H_2O_4$), anhydrous sodium sulfate (Na_2SO_4), ethylene glycol ($C_2H_6O_2$), citric acid ($C_6H_8O_7$), potassium ferricyanide ($K_3Fe(CN)_6$) and potassium ferrocyanide ($K_4Fe(CN)_6$) were obtained from Tianjin Damao Chemical Reagent Co., Ltd. Tin chloride pentahydrate ($SnCl_4 \cdot 5H_2O$), antimony trichloride ($SbCl_3$) and rhodamine B (RhB) were obtained from Aladdin Reagent Co., Ltd. All of the chemicals were reagent grade or higher.

2.2. Porous Ti/SnO$_2$–Sb filter preparation

The substrate tubular porous titanium filters were firstly immersed in NaOH solution (10%, m/m) at 90 °C for 1 h to remove grease, and then etched in boiling oxalic acid (10%, m/m) for 1 h to form a gray surface with uniform roughness. Tubular porous Ti/SnO$_2$–Sb filters were prepared by the sol–gel method using a dip coater (SYDC-200, Shanghai Sanyan Technology Co., Ltd. China). The preparation process involved the following steps: citric acid and ethylene glycol were mixed and agitated at 60 °C until fully dissolved, and then the solution was heated to 90 °C under continuous stirring. A mixture of SnCl$_4$·5H$_2$O and SbCl$_3$ was added to the solution at the molar ratio of 140 : 30 : 9 : 1 (ethylene glycol : citric acid : SnCl$_4$·5H$_2$-O : SbCl$_3$) at 90 °C and the resulting mixture was maintained at 90 °C for 1 h in order to obtain a sol–gel. Finally, the sol–gel solution was used to coat the porous titanium filters through dipping at a rate of 200 μm s^{-1}. After that, the porous titanium filters were dried at 140 °C for 20 min in an oven and sintered to induce the thermal decomposition of the coating at 550 °C for 20 min in a muffle furnace. The above operation was repeated 12 times and the last baking was annealed for 2 h at 550 °C to obtain the tubular porous Ti/SnO$_2$–Sb filters. More information concerning the Ti/SnO$_2$–Sb electrode preparation has been given elsewhere.[27]

2.3. Experimental setup

The experimental setup of the reactive electrochemical filter system is shown in Fig. 1. The tubular porous Ti/SnO$_2$–Sb filter was used as the anode and a stainless steel perforated tube with an outside diameter of 6 mm and a length of 150 mm was used as the inner cathode, which was also used as a water distributor.
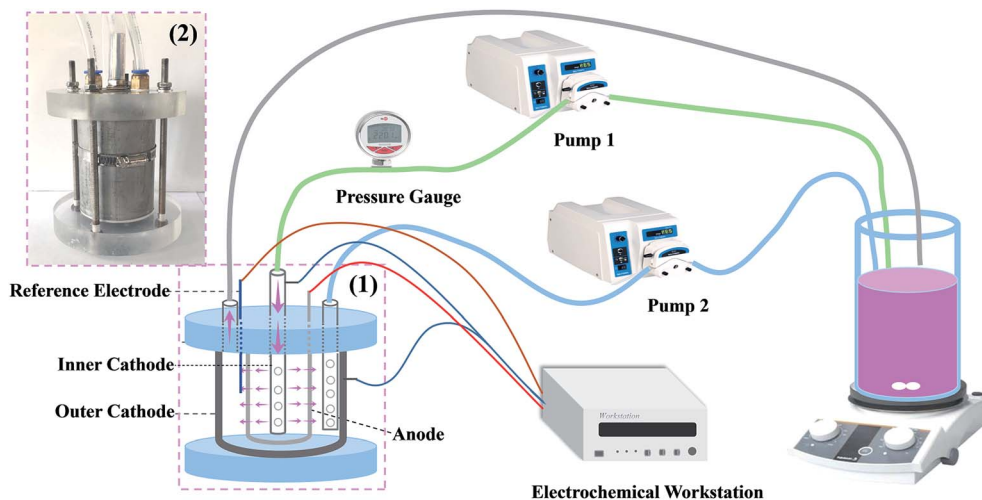
Fig. 1 A schematic diagram of the experimental setup: (1) the design of the reactive electrochemical filter system consisting of two perforated stainless steel pipes acting as water distributors, one of which is also used as the inner cathode, and a stainless steel pipe acting as the outer cathode and a tubular porous Ti/SnO$_2$–Sb filter acting as the anode; (2) a photo of the reactive electrochemical filter system.

A stainless steel tube mold with an inside diameter of 50 mm and a length of 100 mm was used as the outer cathode. The anode and the cathodes were 10 mm apart. The electrochemical workstation (PARSTAT 2273, USA) provided a stable current for the reaction system. In flow-by mode, pump 2 was turned on and pump 1 was turned off; the solution flowed only by the surface of the electrode and then out of the reactor. In flow-through mode, pump 1 was on and pump 2 was off; the solution flowed from the inside of the electrode to the outside of the reactor after passing through the electrode.

2.4. Electrode characterization

The surface morphology of the electrode was characterized by scanning electron microscopy (SEM, Hitachi S-4800, Japan). The crystalline phases of the electrode were measured by X-ray diffraction (XRD, Rigaku D/max-3C, Japan) with Cu Kα radiation at a scanning rate of 2° min^{-1} in 2θ mode from 20° to 80°. The surface composition of the electrode was characterized by X-ray photoelectron spectroscopy spectra (XPS, ESCALAB 250Xi, USA) with a monochromatic Al Kα source. The pore size distributions and porosity of the electrode were characterized by mercury porosimetry (AutoPore IV 9500, Micromeritics). The pressure–membrane flux relation was calculated according to the different inlet flow and corresponding pressure values in flow-through mode. The linear sweep voltammetry (LSV) scanning and cyclic voltammetry (CV) scanning were carried out on the system in flow-through mode and were driven by an electrochemical workstation (PARSTAT 2273, USA), with a tubular porous Ti/SnO$_2$–Sb filter as the working electrode, two stainless steel tubes as the counter electrode and a saturated calomel electrode (SCE) as the reference electrode.

2.5. Electrochemical experiments

The electrochemical experiments were performed using the setup shown in Fig. 1. The normalized mass transfer rate

constant (k_m, m s^{-1}) for the pollutant diffusion to the electrode surface in flow-through mode was characterized using the electrooxidation rate constant of Fe(CN)$_6^{4-}$, in which oxidation only occurred on the anode surface through direct electron transfer (for details, see Text S1†). In this experiment, 2 L of 0.1 M KH$_2$PO$_4$ with 5 mM K$_4$Fe(CN)$_6$ and 1 mM K$_3$Fe(CN)$_6$ solution was continuously flowed and recirculated in flow-through mode.

The electrochemical degradation of RhB was conducted using a 1 L solution containing 50 mM Na$_2$SO$_4$ and 50 mg L^{-1} RhB in the reactive electrochemical filter system at an inlet flow rate of 1.8 L min^{-1}. Both the feed and permeate streams were 100% recycled for 10 min to purge the system at zero current, then an input current between 0.25 A and 1.5 A was applied to the reactive electrochemical filter system. Triplicate samples of 5 mL each were taken at different time intervals. During each sampling, the electrolysis was stopped and the solution was kept looping to ensure the solution was homogeneous. All of the electrolysis experiments were triplicated and carried out at room temperature (25 ± 1 °C). The corresponding results were averaged with a standard deviation below 10% of the means.

2.6. Analytical methods

The concentrations of RhB and Fe(CN)$_6^{3-}$ were determined by UV-vis spectrophotometry (UV-5100B, Shanghai Yuanxi Analysis Instrument Co., Ltd. China) at the wavelengths of 553 and 420 nm, respectively. The total organic carbon (TOC) was measured by a TOC analyzer (TOC-L CPH, Shimadzu Co., Ltd. Japan).

The RhB degradation rate (η, %) was calculated according to the following equation:

$$\eta = \frac{C_0 - C_t}{C_0} \times 100\% \tag{1}$$

where C_0 (mg L^{-1}) and C_t (mg L^{-1}) are the concentrations at time zero and time t, respectively. The RhB oxidation flux (OF, mol h^{-1} m^{-2}) was calculated according to the following equation:[28]

$$\text{OF} = \frac{C_0 - C_t}{At} V \qquad (2)$$

where A (m^2) is the geometric surface area of the anode, V (m^3) is the reaction volume and t (h) is the reaction time. The reaction time (t, h) was calculated according to the following equation:

$$t = \frac{1}{k_{\text{RhB}}} \ln \frac{C_0}{C_t} \qquad (3)$$

where k_{RhB} is the pseudo-first-order kinetic constant of RhB oxidation. The overall mineralization current efficiency (MCE, %) was calculated according to the following equation:

$$\text{MCE}(\%) = \frac{n}{28} \frac{\Delta\text{TOC}}{12I\Delta t} FV \times 100\% \qquad (4)$$

where ΔTOC is the concentration of TOC (g L^{-1}) removed during a given electrolysis time (Δt, s), I is the input current (A), F is the Faraday constant (96 485C mol^{-1}), V is the treatment solution volume (L), and $n = 156$ is the electron number required to completely mineralize one molecule of RhB, and $n = 28$ and $n = 12$ are the number of carbon atoms contained in each RhB molecule and the atomic mass of carbon, respectively. The electrical energy consumption, EE/O, was calculated to evaluate the energy efficiency of the reactive electrochemical filter system. The EE/O is defined as the energy required to reduce the concentration of the target pollutant by one order of magnitude. The EE/O (kW h m^{-3}) was calculated according to the following equation:[29]

$$\text{EE/O} = \frac{U_{\text{cell}}I}{V} t_{90\%} \qquad (5)$$

where U_{cell} is the average cell voltage applied during the treatment (V), I is the input current (A), $t_{90\%}$ is the time required for 90% RhB degradation (h), and V is the treatment solution volume (L).

3. Results and discussion

3.1. Physical characterization

The photos and SEM images of the substrate, sintered powder porous tubular titanium filter, and the fabricated porous Ti/SnO$_2$–Sb filter are shown in Fig. 2. As shown in Fig. 2(a), the surface of the substrate after cleaning and corrosion treatment appears very rough, which contributes to the coating by the sol precursor solution. After the sol–gel preparation process, the Ti/SnO$_2$–Sb filter maintained its highly porous structure, and the size of the aperture did not appear to change significantly (see Fig. 2). From the enlarged view in Fig. 2(b), we can observe that the Sb-doped SnO$_2$ coating on the surface of the porous Ti/SnO$_2$–Sb filter is compacted and crack-free, which helps prolong the service life of the porous Ti/SnO$_2$–Sb filter.[28]

Fig. 2(c) shows the wide-angle XRD analysis of the substrate and the fabricated porous Ti/SnO$_2$–Sb filter. A series of diffraction peaks for the titanium metal and SnO$_2$ structures were

recorded using the fabricated porous Ti/SnO$_2$–Sb filter. Diffraction peaks for Sb and its oxide were not observed, however Fig. 2(d) shows the presence of Sb in the porous Ti/SnO$_2$–Sb filter. Therefore, we infer that Sb is well-dispersed in the SnO$_2$ lattice and forms a Sb-doped SnO$_2$ solid solution.[30] Compared with the standard card (JCPDS card no: 41-1445), the Sb-doped SnO$_2$ coating film is identified as a rutile-type crystal. Additionally, no crystallized TiO$_2$ diffraction peak was found, which strongly suggested that the titanium support substrate is not oxidized during the Sb-doped SnO$_2$ coating film preparation.

The pore structure and pore size distribution were characterized more thoroughly using Hg intrusion porosimetry as is shown in Fig. 2(e). The intrusion pore volumes of the substrate and the Ti/SnO$_2$–Sb filter were almost unchanged, which was attributed to the macropores of 6–60 μm. The median pore diameters (based on volume) of the substrate and the Ti/SnO$_2$–Sb filter were 31.5 μm and 30.2 μm, respectively. The median pore diameter (based on volume) of the Ti/SnO$_2$–Sb filter was 31.5 μm, slightly larger than that of the substrate (30.2 μm). This is mainly caused by oxalic acid corrosion during the substrate pre-treatment.

Penetration flux is an important indicator for the performance of porous membrane-like materials, and it was used to characterize the permeability of the porous Ti/SnO$_2$–Sb filter. The pressure–membrane flux relationship is shown in Fig. 2(f). Due to the similar pore diameters of the substrate and the porous Ti/SnO$_2$–Sb filter, the pure water membrane flux of the substrate and the porous Ti/SnO$_2$–Sb filter is almost the same (see Fig. 2(e)). The pure water penetration flux of the porous Ti/SnO$_2$–Sb filter is as high as 61.94 m^3 m^{-2} h^{-1} bar^{-1}, thus both the permeability and water treatment capacity are superior compared with the reactive electrochemical membranes reported in the literature, including Ti$_n$O$_{2(n-1)}$ conductive ceramic membranes (0.05 m^3 m^{-2} h^{-1} bar^{-1} to 3.21 m^3 m^{-2} h^{-1} bar^{-1})[13,27,31] and CNT-networks (0.017 m^3 m^{-2} h^{-1} to 0.34 m^3 m^{-2} h^{-1}).[14] As a result, the reactive electrochemical filter system in this work can maintain a high water flux under low-pressure conditions, which makes it easy to operate during water treatment.

3.2. Electrochemical characterization

The linear polarization curves of the porous Ti/SnO$_2$–Sb filter are displayed in Fig. 3(a) and the measured oxygen evolution potentials (OEP) are 1.74 V and 1.87 V (vs. SCE) in neutral and acidic conditions, respectively. The high oxygen evolution over-potential indicated a low side reaction of oxygen formation, which would be beneficial for promoting the oxidation efficiency of pollutants during electrocatalytic oxidation processes. Therefore, the electrode has a better electrochemical performance in acidic conditions.

The cyclic voltammetry (CV) curves of the porous Ti/SnO$_2$–Sb filter in 0.5 M Na$_2$SO$_4$ solution and 0.5 M Na$_2$SO$_4$ solution with 10 mg L^{-1} RhB were generated to investigate the reaction type of RhB degradation in the reactive electrochemical filter system in this study. As shown in Fig. 3(b), no additional peaks were
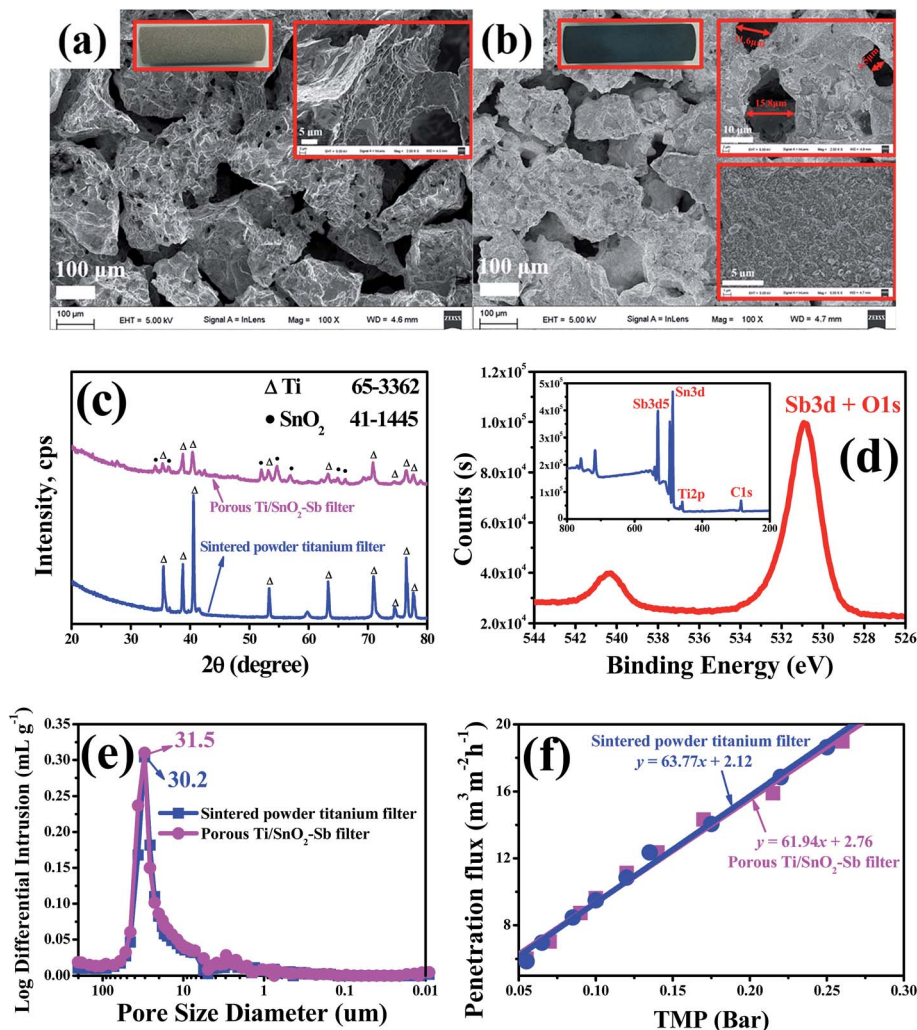
Fig. 2   SEM images: (a) the substrate and tubular sintered powder porous titanium filter; (b) the fabricated porous Ti/SnO$_2$−Sb filter; (c) XRD patterns; (d) XPS analysis; (e) the results of the Hg intrusion porosimetry analysis of the pore size distribution; (f) the pure water penetration flux of the substrate and porous Ti/SnO$_2$−Sb filter.

found in Na$_2$SO$_4$ with RhB solution compared to the CV curve recorded in Na$_2$SO$_4$ solution, indicating that the direct electro-oxidation of RhB over the porous Ti/SnO$_2$−Sb filter did not occur.[21] Obviously, we can conclude that an indirect ˙OH attack

plays a key role in the RhB electrooxidation process in flow-through mode.

The electrochemical stability of the tubular porous Ti/SnO$_2$−Sb filter was also evaluated. Fig. S1† shows the results of the
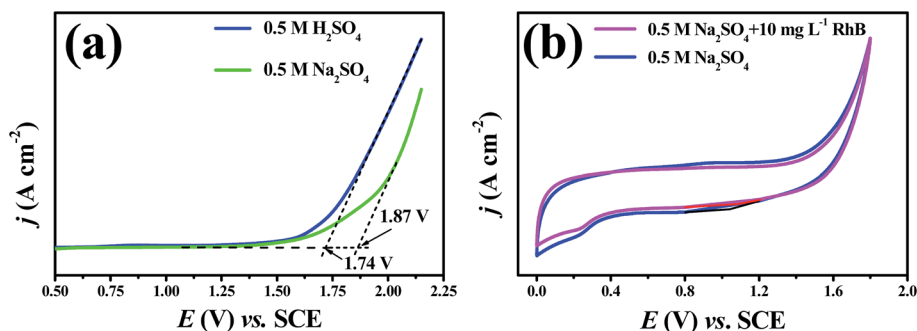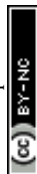

Fig. 3   (a) The linear polarization curves and (b) cyclic voltammetry curves of the porous Ti/SnO$_2$−Sb filter at a scan rate of 50 mV s^{-1}. Penetration flux: 12.3 m^3 m^{-2} h^{-1}.

accelerated service life test on the porous Ti/SnO$_2$–Sb filter at a current density of 0.5 A cm^{-2} in 0.5 M H$_2$SO$_4$ solution at 30 °C. It was observed that the accelerated service life time was about 10.23 h when the cell voltage increased from 5 V to 10 V. The actual service life can be calculated by the following equation:

$$\tau_1 = \left(\frac{I_2}{I_1}\right)^2 \tau_2 \qquad (6)$$

where I_1 (A m^{-2}) and I_2 (A m^{-2}) are the actual current density and the accelerated current density, respectively. τ_1 (h) and τ_2 (h) are the actual service life time and the accelerated service life time, respectively. The actual service life of the porous Ti/SnO$_2$– Sb filter was 2.92 years under a current density of 10 mA cm^{-2}. Compared with previous studies (as shown in Table S1†), the service life of the porous Ti/SnO$_2$–Sb filter in this study was much longer. The improved service life was probably attributed to the use of porous materials, which are conductive and could tightly combine the Sb-doped SnO$_2$ coating layer with the substrate.[32]

The electrochemically active surface area is where active sites are accessible to the electrolyte when the electrochemical reaction occurs.[33] Voltammetric charge (q^*), which is closely related to the real surface area and the number of electro-active sites on an electrode (especially for a porous electrode), is a major factor for determining the electrochemical performance of an electrode.[34–36] The CV curves of the tubular porous Ti/ SnO$_2$–Sb filter electrode, performed within the potential range of 0.4 V to 1.2 V *vs.* SCE in 0.5 M Na$_2$SO$_4$ solution in flow-through mode at different sweep rates as shown in Fig. S2(a),† are used to calculate the q^* by integrating the CV over the whole potential range to further calculate the electrochemical porosity and roughness factor (R_f) (for details, see Text S2, Fig. S2(b) and S2(c)†).

The values of the charges, electrochemical porosity, and R_f are calculated and listed in Table S2.† As shown in Table S2,† the electrochemical porosity and R_f of the porous Ti/SnO$_2$–Sb filter are 73.3% and 1428.2 ± 37.2, respectively. These values for the electrochemical porosity and roughness factor indicate that the porous Ti/SnO$_2$–Sb filter is three-dimensional in nature, and hence could provide large numbers of active sites for electro-catalytic oxidation.

3.3. The mass transfer performance of the reactive electrochemical filter system

To investigate the mass transfer performance of the reactive electrochemical filter system in flow-through mode, the kinetics of Fe(CN)$_6$$^{4-}$ oxidation (k_{obs}) were measured as a function of penetration flux (J, m s^{-1}). It should be noted that the penetration flux of the porous Ti/SnO$_2$–Sb filter is extremely high, *i.e.* 61.94 m^3 m^{-2} h^{-1} bar^{-1}. Such a high flux means that the permeability of the porous Ti/SnO$_2$–Sb filter is pretty good and even gravity flow can be achieved. The penetration fluxes tested in this study are also very high (up to 5.17 × 10^{-3} m s^{-1} or 18.6 m^3 m^{-2} h^{-1}), tens to hundreds of times higher than that reported in the previous literature.[13,14,27,30] As shown in Fig. 4, it is very interesting that the k_{obs} values were plateauing at around
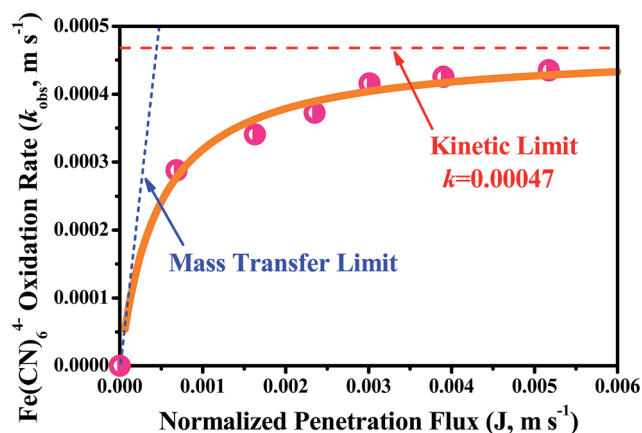

Fig. 4 A plot of the normalized observed rate constant (k_{obs}, m s^{-1}) for Fe(CN)$_6$$^{4-}$ oxidation in the reactive electrochemical filter system operated in flow-through mode as a function of penetration fluxes (J, m s^{-1}). The solid orange line represents eqn (7), the model fit, the red dashed line is the normalized kinetic rate constant (k, m s^{-1}) estimated by model fit to experimental data, and the blue dotted line is the convective mass transfer limit calculated by $k_{obs} = J$. Experimental solution: 2 L of 0.1 M KH$_2$PO$_4$ with 5 mM K$_4$Fe(CN)$_6$ and 1 mM K$_3$Fe(CN)$_6$ solution.

4.2 × 10^{-4} m s^{-1} and at a penetration flux greater than 3.01 × 10^{-3} m s^{-1}, the k_{obs} values only increased by 4.5% when the penetration fluxes were enhanced by 1.72 times from 3.01 × 10^{-3} m s^{-1} to 5.17 × 10^{-3} m s^{-1} (or 10.8–18.6 m^3 m^{-2} h^{-1}). These results strongly suggest that the Fe(CN)$_6$$^{4-}$ oxidation process at very high penetration fluxes is controlled by kinetic limitation rather than mass transfer. To the best of our knowledge, the measured k_{obs} value (4.35 × 10^{-4} m s^{-1}) in this study is the highest in an electrochemical flow-through reactor compared with those reported in the literature. The measured k_{obs} values were 3.1-fold and 4.4-fold higher than the highest value reported for Ti$_4$O$_7$-based reactive electrochemical membranes (1.4 × 10^{-4} m s^{-1})[13] and CNT network based reactive electrochemical filters (1.0 × 10^{-4} m s^{-1})[37]. More contrastive details are shown in Table S3.†

Fitting the measured k_{obs} values with eqn (S4)† yielded a value of $k = (4.7 \pm 0.08) \times 10^{-4}$ m s^{-1}, which is the assumed kinetic limit. Our k value is 2.8 times higher than the value reported by Chaplin (1.7 × 10^{-4} m s^{-1}) who used a Ti$_4$O$_7$-based reactive electrochemical ultrafiltration membrane[13]. This is mainly attributable to the great roughness factor (R_f = 1428.2 ± 37.2) of the Sb-doped SnO$_2$ coating layer, which was much higher than that of the Ti$_4$O$_7$-based reactive electrochemical ultrafiltration membrane (R_f = 246.3 ± 11.4), which provided much more electrochemical reactive sites. A conservative estimation of the boundary diffusion length (δ) was calculated by $\delta = D/k$, where $D = 7.6 \times 10^{-10}$ m^2 s^{-1} is the water diffusion coefficient for Fe(CN)$_6$$^{3-}$. Based on $k = 4.7 \pm 0.08 \times 10^{-4}$ m s^{-1} a value of $\delta = 1.6$ μm was estimated, which is much lower than the average pore radius (about 15 μm). These results support the hypothesis that the reactive electrochemical filter system with the porous Ti/SnO$_2$–Sb filter, with excellent water permeability, developed in this study could greatly improve the mass transfer

of the electrochemical process by reducing the thickness of the boundary diffusion layer. Additionally, these results also suggest that for further improvement of the intrinsic kinetic reactivity of the reactive electrochemical filter system, it is necessary to design new electrode materials with higher specific electroactive surface area or roughness.

3.4. Electrooxidation performance of the reactive electrochemical filter system

3.4.1 The effect of flow-by and flow-through modes on RhB oxidation.

To determine the potential of the reactive electrochemical filter system developed in this study (see Fig. 1) for water treatment applications, a series of experiments for RhB oxidation were performed in both flow-by and flow-through modes using 1 L solution containing 50 mM Na_2SO_4 and 50 mg L^{-1} RhB at 0.5 A constant input current with the same inlet flow of 1.8 L min^{-1}. The solutions were 100% recycled to the feed reservoir in order to characterize the RhB decay kinetics and TOC removal. As presented in Fig. 5, the reactive electrochemical filter exhibited a remarkable oxidation efficiency in flow-through mode compared with that in flow-by mode, e.g., >99% RhB decay rate and 51% TOC removal were achieved at 20 min in flow-through mode. While in flow-by mode, only 58.8% RhB decay rate and 8.8% TOC removal after 30 min treatment were observed. The change in RhB concentration in both flow-through mode and flow-by mode can be well fitted by a pseudo-first-order model, based on which the half-life ($t_{1/2}$) values (see Table 1) were calculated as 2.9 min and 25.3 min for flow-through mode and flow-by mode, respectively. As expected, the pseudo-first-order kinetic constant (k_{RhB}) of flow-through mode is 0.235 min^{-1}, which is 8.6 times higher than that of flow-by mode (0.0274 min^{-1}), clearly showing that the mass transfer of RhB molecules from the bulk solution to the anode surface was much faster in flow-through mode. Furthermore, there was very little TOC decay in flow-by mode. However continuous rapid decay of TOC in flow-through mode was observed with a TOC removal value of 52.5% after 30 min of treatment, indicating that significant mineralization of RhB occurred. These results strongly confirm that the reactive electrochemical filter system constructed in this study achieves an outstanding oxidation efficiency when operating in flow-through mode by improving the mass transfer rates of pollutants from the bulk solution to the filter surface. This treatment system has great potential to bring down the high cost of the traditional electrooxidation water treatment technology, in investment and operation.

3.4.2 The effect of anode potential (E) in flow-through mode on RhB oxidation.

The applied anode potential is a key parameter, which affects the capability of 'OH generation on the anode surface in the electrooxidation process. Meanwhile, the correct anode potential has a positive impact on energy saving. Therefore, the effect of anode potentials on the degradation of RhB was investigated to further evaluate the electrooxidation performance in flow-through mode. The reactivity of the reactive electrochemical filter system for a 1 L solution containing 50 mM Na_2SO_4 and 50 mg L^{-1} RhB was characterized at various applied anode potentials (1.94 V to 3.04 V vs. SCE). The system was operated in flow-through mode at a penetration flux of 12.3 m^3 m^2 h^{-1}, and solutions were 100% recycled to the feed reservoir. The RhB decay rate and TOC removal results of the individual experiments are shown in Fig. 6, and the corresponding kinetics parameters of the pseudo-kinetic order are summarized in Table 1. The oxidation efficiency of RhB was positively correlated with the applied anode potential. For example, the RhB decay rate (k_{RhB}, min^{-1}) approximately doubled upon raising the potential from 1.94 to 2.18 V vs. SCE, with k_{RhB} values of 0.135 min^{-1} at 1.94 V vs. SCE and 0.235 min^{-1} at 2.18 V vs. SCE. However, the k_{RhB} value increased by only 30% to 0.304 min^{-1} when the anode potential was raised from 2.18 V to 3.04 V vs. SCE, which indicated that the rate of the k_{RhB} increment will no longer be significant with the further improvement of the anode potential. This phenomenon is predictable because the reactive electrochemical filter system in flow-through mode at a very high penetration flux, 12.3 m^3 m^2 h^{-1}, might be under kinetic limitation as revealed in Section 3.3. In addition, the yield of 'OH also increased linearly with the anode potential at high anode potentials, being much higher than the oxygen evolution potential of the electrode.[38] Moreover, an excessively high electrode potential led to a water discharge occurring violently with the generation of a larger amount of oxygen and hydrogen microbubbles, which impeded
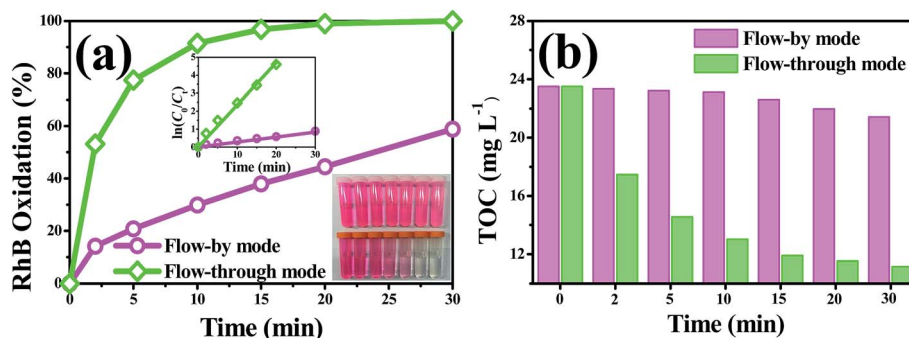

Fig. 5 Comparison of the electroxidation efficiency of RhB in flow-by mode and flow-through mode under the same conditions (RhB concentration: 50 mg L^{-1}; input current: 0.5 A; pH = 7; supporting electrolyte: 50 mM Na_2SO_4; flow rate/penetration flux: 1.8 L min^{-1} or 12.3 m^3 m^2 h^{-1}): (a) decay kinetics, and (b) TOC removal.

Table 1 Summary of results for the RhB electrooxidation experiments operated in flow-by or flow-through mode

Operating mode	Input current (A)	Average cell voltage (V)	Anode potential (V vs. SCE)	RhB oxidation at 30 min	Pseudo-first-order rate constants (k_{RhB}, min^{-1})	R^2	Half-life ($t_{1/2}$, min)	$t_{90\%}$ (min)^a	Observed rate constant ($k_{obs, RhB}$, m s^{-1})^b	Mineralization current efficiency (MCE) at 30 min	Energy consumption (EE/O, kW h m^{-3})
Flow-by	0.5	3.5	2.25	58.8%	0.0274	0.992	25.3	84.0	0.53×10^{-4}	9.6%	2.45
Flow-through	0.25	3.0	1.94	97.6%	0.135	0.994	5.1	17.1	3.01×10^{-4}	104.1%	0.21
Flow-through	0.5	3.4	2.18	>99.9%	0.235	0.994	2.9	9.8	4.65×10^{-4}	57.5%	0.28
Flow-through	1.5	4.2	3.04	>99.9%	0.304	0.975	2.3	7.6	5.76×10^{-4}	19.2%	0.82

^{a} $t_{90\%}$ is the time required for 90% RhB degradation (h). ^{b} $k_{obs, RhB}$ is calculated by eqn (S3).†

the oxidation of RhB. A similar decay trend for the TOC removal was also observed, and the TOC removal values were 47.5%, 52.5%, and 52.7% for 1.94 V, 2.18 V, and 3.04 V vs. SCE, respectively, after 30 min of treatment. In addition, it is worth noting that RhB oxidation in flow-through mode reached an observed rate constant ($k_{obs, RhB}$, m s^{-1}) of 5.76×10^{-4} m s^{-1} at an anode potential of 3.04 V vs. SCE (~8.5 mA cm^{-2}) (see Table 1), which is much higher than the highest rate constants observed in the reactive electrochemical filter systems in flow-through mode with carbon nanotube and/or Ti$_4$O$_7$ (1.7×10^{-5}–1.4×10^{-4} m s^{-1}) reported in the literature to date.[14,39–41] Once again, these results demonstrate the benefit of the reactive electrochemical filter system in flow-through mode using a porous Ti/SnO$_2$–Sb filter with an excellence penetration flux.

3.5. The RhB oxidation flux, mineralization current efficiency and mechanism

To better understand the oxidative capacity of the system with the porous Ti/SnO$_2$–Sb filter and to better facilitate the design of reactive electrochemical filter water treatment systems, the RhB oxidation flux (OF, mol h^{-1} m^{-2}) was calculated using eqn (2), similar to the membrane flux. The RhB oxidation flux was examined as a function of the operating mode and anode potential, as displayed in Fig. 7(a). As expected, it was observed that the RhB oxidation flux in flow-through mode was much higher than that in flow-by mode. For a 99% RhB oxidation, an oxidation flux value of 0.033 mol m^{-2} h^{-1} was achieved in flow-through mode at an anode potential of 2.18 V vs. SCE, approximately 8.5 times higher than that in flow-by mode (0.0039 mol m^{-2} h^{-1}) under the same experimental conditions. This is mainly due to the excellent mass transfer performance in flow-through mode, resulting in the rapid diffusion of RhB molecules towards the anode surface reaction zone. RhB molecules are thus able to react with the ˙OH generated by the porous Ti/SnO$_2$–Sb filter. Additionally, the oxidation flux increased with the increasing anode potential in flow-through mode. At an anode potential of 3.04 V vs. SCE, about 99% of 0.10 mM (50 mg L^{-1}) RhB was oxidized with an oxidation flux of 0.044 mol m^{-2} h^{-1}, which was about 1.8 times higher than the value for tetracycline (0.2 mM) reported by Liu (0.024 mol h^{-1} m^{-2}) who used a CNT reactive electrochemical filter in flow-through mode.[28] More contrastive information is shown in Table S4.†

As shown in Fig. 7(b) and Table 1, the overall mineralization current efficiencies (MCEs) for RhB over the entire electrolysis process of 30 min were 104.1%, 57.5%, and 19.2% in flow-through mode at anode potentials of 1.94, 2.18, and 3.04 V vs. SCE, respectively, while it was only 9.6% in flow-by mode at an anode potential of 2.18 V vs. SCE, which is similar to the value (about 10%) reported by others using traditional parallel plate electrode systems.[42] At an anode potential of 2.18 V vs. SCE, the overall mineralization current efficiency was calculated to be 83.6% with 99% RhB oxidation and ~51% TOC removal. It is noteworthy that the mineralization current efficiency in flow-through mode was greater than 100% over the first several minutes of operation, e.g., the MCEs were 49.1%, 146.3%, and
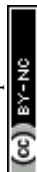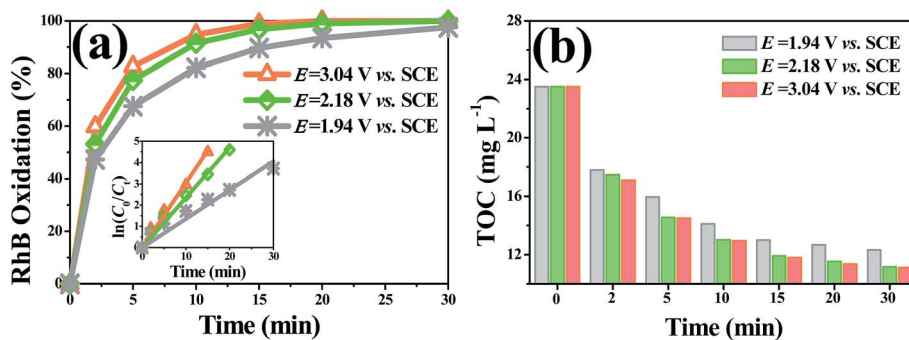
Fig. 6 The effect of anode potential on the electrooxidation efficiency of RhB in flow-through mode (RhB concentration: 50 mg L^{-1}; pH = 7; supporting electrolyte: 50 mM Na$_2$SO$_4$; penetration flux: 12.3 m^3 m^2 h^{-1}): (a) decay kinetics, and (b) TOC removal.
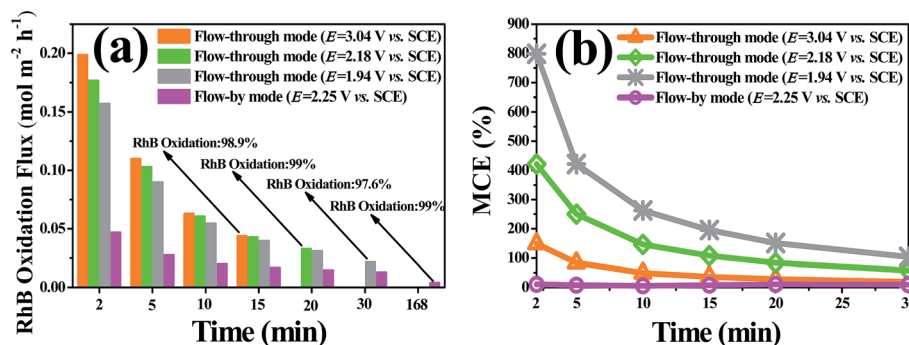

Fig. 7 (a) The RhB oxidation flux and (b) the overall mineralization current efficiency (MCE) vary with treatment time. The experimental conditions are the same as in Fig. 5 and 6.

262.5%, respectively, in the first 10 min of electrolysis at anode potentials of 3.04, 2.18, and 1.94 V vs. SCE, respectively. Due to the fact that the reactive electrochemical filter system in flow-through mode was suffering from severe kinetic limitation, the ˙OH concentration was not sufficient for RhB to be completely mineralized to CO$_2$ at a low anodic potential. Thus, the MCE being over 100% may be mainly attributable to part of the aromatic phenol intermediates produced by RhB oxidation being electro-polymerized to form polymers by direct electron transfer, which further aggregate to form macromolecules and are trapped or adsorbed onto the filter anode surface or precipitated. The observation of an anode potential of 1.94 V vs. SCE also supports the hypothesis that a layer of very sparse yellow substance was attracted to the surface of the porous Ti/SnO$_2$–Sb filter after electrooxidation.

The oxidation mechanism of RhB by ˙OH has been studied in detail previously.[43,44] It is recognized that two competitive processes occur simultaneously during the ˙OH attraction: the N-deethylation and destruction of the dye chromophore structure (a conjugated xanthene ring). In our case, there was no obvious shift in the characteristic absorption bands but a sharp reduction was observed as shown in Fig. 8, which proved that the decomposition of the conjugated xanthene ring was the dominant oxidation pathway for RhB. The open-ring reaction of the conjugated xanthene will generate a series of aromatic phenol intermediates, such as o-phenylphenol, 2,3-dihydroxybenzoic acid, 2,5-hydroxybenzoic acid, 3-hydroxybenzoic acid,

(iso/tere)-phthalic acid and benzoic acid, which have been detected in the previous literature.[43–47] These compounds were further degraded into smaller aliphatic acids and were eventually completely mineralized to CO$_2$, which can be proved by the results of the TOC measurement. Moreover, some of the aromatic phenol intermediates such as o-phenylphenol and 2,3-
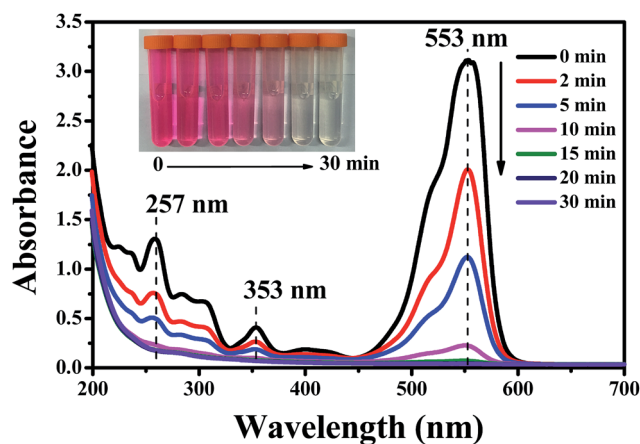

Fig. 8 The UV-vis spectrum of the RhB solution at various time intervals for the reactive electrochemical filter system in flow-through mode with an applied anode potential of 2.18 V vs. SCE. Experimental conditions: RhB concentration: 50 mg L^{-1}; pH = 7; supporting electrolyte: 50 mM Na$_2$SO$_4$; penetration flux: 12.3 m^3 m^2 h^{-1}.
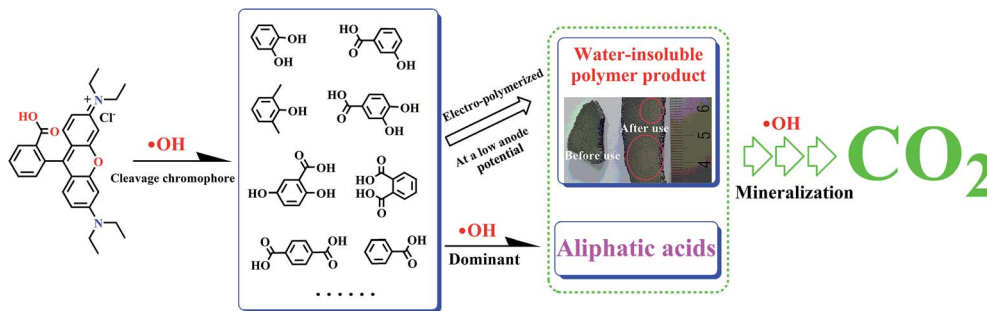
Fig. 9 A schematic diagram illustrating the RhB mineralization mechanism.

dihydroxybenzoic acid are capable of forming polymers over the anode surface at a low anode potential such as 1.94 V *vs.* SCE. On the basis of all of the above experimental results and the previous studies, a simple schematic to describe the RhB oxidation process in the reactive electrochemical filter system in this study is given in Fig. 9.

3.6. Energy consumption

Energy consumption is an important factor to consider when evaluating the application prospects of the reactive electrochemical filter system with the porous Ti/SnO_2–Sb filter developed in the present study for wastewater treatment. The electrical efficiency per log order degradation (EE/O, kW h m^{-3}) of RhB was calculated to evaluate the economic feasibility of the reactive electrochemical filter system and is shown in Table 1. The energy demand of the reactive electrochemical filter system in flow-through mode increases with the increase in the applied anode potential, and the system in flow-through mode exhibited a much lower energy consumption than that in flow-by mode under the same conditions. The EE/O value was 0.28 kW h m^{-3} in flow-through mode at an anode potential of 2.18 V *vs.* SCE, which was only 11.43% of that in flow-by mode at an anode potential of 2.25 V *vs.* SCE (2.45 kW h m^{-3}). The EE/O values were 0.21 kW h m^{-3} and 0.82 kW h m^{-3}, respectively, at anode potential values of 1.94 V and 3.04 V *vs.* SCE in flow-through mode. Notably, the EE/O value was increased by 3.9 times, while the k_{RhB} value was only enhanced by 2.25 times when the anode potential increased from 1.94 V to 3.04 V *vs.* SCE, indicating that a higher anode potential led to a lower energy efficiency. However, the evaluation of a system depends not only on the energy consumption, but also on the space efficiency. The residence time values ($t_{90\%}$) were 17.1 min, 9.8 min and 7.8 min at the anode potentials of 1.94 V, 2.18 V and 3.04 V *vs.* SCE, respectively. In view of the appreciable space efficiency and energy consumption, the anode potential of 2.18 V *vs.* SCE was a good choice due to the low energy consumption (0.28 kW h m^{-3}, or 97.2 kW h per kg TOC at ~44% TOC removal) and the relatively short residence time (9.8 min). The value of 97.2 kW h per kg TOC (equal to 36.4 kW h per kg COD in theory) was much lower than the value reported by Yang[48] (101.34 kW h kg COD^{-1}) who used a CNT flow-through reactor for the degradation of reactive Brilliant red X-3B (50 mg L^{-1}) with ~82% oxidation removal and ~46% COD

removal. Alternatively, the value of 0.28 kW h m^{-3} is comparative to the state-of-the-art electrochemical oxidation processes with energy consumptions in the range of 0.1–40 kW h m^{-3}.[28]

4. Conclusions

The major conclusions drawn from this study are summarized as follows.

(1) Tubular porous Ti/SnO_2–Sb filters were prepared by a sol–gel method using low-cost powder sintered porous titanium filters with an average pore size of about 30 μm as the substrates. These porous Ti/SnO_2–Sb filters exhibited excellent penetration fluxes (up to 61.94 m^3 m^{-2} h^{-1} bar^{-1}) and good electrochemical properties, such as high oxygen evolution potentials, electrochemical stability and high electro-active surfaces.

(2) A convection-enhanced rate constant for $Fe(CN)_6^{4-}$ oxidation of 4.35×10^{-4} m s^{-1} was achieved at a high penetration flux of 18.6 m^3 m^{-2} h^{-1}, which approached the kinetic limit and is the highest reported in a reactive electrochemical filter system. The results also suggested that for further improvement of the intrinsic kinetic reactivity of the reactive electrochemical filter system, it is necessary to design new electrode materials with higher specific electroactive surface area or roughness.

(3) The reactive electrochemical filter system in flow-through mode resulted in a 8.6-fold enhancement in the observed first-order rate constant for RhB oxidation (k_{RhB}, min^{-1}) relative to flow-by mode at an input current of 0.5 A (~2.8 mA cm^{-2}). RhB oxidation in flow-through mode reached an observed rate constant ($k_{obs, RhB}$, m s^{-1}) of 5.76×10^{-4} m s^{-1} at an anode potential of 3.04 V *vs.* SCE (~8.5 mA cm^{-2}), which is much higher than the highest rate constants reported in the literature to date (1.7×10^{-5}–1.4×10^{-4} m s^{-1}).

(4) The mineralization current efficiency in flow-through mode was more than one magnitude higher than that in flow-by mode under the same experimental conditions. Under an anode potential of 2.18 V *vs.* SCE, the electrical energy per order degradation (EE/O) for RhB was as low as 0.28 kW h m^{-3} in flow-through mode, with a relatively short residence time of 9.8 min. This value is comparative to the state-of-the-art electrochemical oxidation processes with energy consumptions in the range of 0.1–40 kW h m^{-3}.
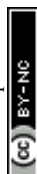
These anodic reactive electrochemical membranes, the porous Ti/SnO$_2$–Sb filters, are low-cost and easy to mass-produce. In this study, we developed a reactive electrochemical filter system that is practical and can be implemented for large-scale industrial applications and has a high penetration flux, a high mass transfer rate and a strong electrooxidation performance. It is a promising technology for treating organics in wastewater. Further investigations into the toxicity as well as the effects of the matrix and operation parameters should be carried out before applying this technology to wastewater purification.

Conflicts of interest

The authors declare no competing financial interest.

Acknowledgements

References

1 G. Chen, *Sep. Purif. Technol.*, 2004, **38**, 11.

2 E. S. Z. El-Ashtoukhy, N. K. Amin and O. Abdelwahab, *Chem. Eng. J.*, 2009, **146**, 205.

3 H. Yu, Y. Li, M. Zhao, H. Dong, H. Yu, S. Zhan and L. Zhang, *Catal. Today*, 2015, **258**, 156.

4 X. Li, Y. Wu, W. Zhu, F. Xue, Y. Qian and C. Wang, *Electrochim. Acta*, 2016, **220**, 276.

5 E. Tsantaki, T. Velegraki, A. Katsaounis and D. Mantzavinos, *J. Hazard. Mater.*, 2012, **207**, 91.

6 A. Fernandes, D. Santos, M. J. Pacheco, L. Ciriaco and A. Lopes, *Sci. Total Environ.*, 2016, **541**, 282.

7 F. C. Moreira, J. Soler, A. Fonseca, I. Saraiva, A. R. B. Rui, E. Brillas and V. J. P. Vilar, *Appl. Catal., B*, 2016, **182**, 161.

8 J. Niu, H. Lin, J. Xu, H. Wu and Y. Li, *Environ. Sci. Technol.*, 2012, **46**, 10191.

9 Q. Zhuo, M. Luo, Q. Guo, G. Yu, S. Deng, Z. Xu, B. Yang and X. Liang, *Electrochim. Acta*, 2016, **213**, 358.

10 B. P. Chaplin, *Environ. Sci.: Processes Impacts*, 2014, **16**, 1182.

11 H. Lecher and W. Siefken, *Electrochim. Acta*, 2009, **54**, 2018.

12 A. Donaghue and B. P. Chaplin, *Environ. Sci. Technol.*, 2013, **47**, 12391.

13 L. Guo, Y. Jing and B. P. Chaplin, *Environ. Sci. Technol.*, 2016, **50**, 1428.

14 M. H. Schnoor and C. D. Vecitis, *J. Phys. Chem. C*, 2013, **117**, 2855.

15 A. Kitada, G. Hasegawa, Y. Kobayashi, K. Kanamori, K. Nakanishi and H. Kageyama, *J. Am. Chem. Soc.*, 2012, **134**, 10894.

16 S. E. Elsherif, D. B. Bejan and N. J. B J Bunce, *Can. J. Chem.*, 2010, **88**, 928.

17 D. Bejan and N. J. Bunce, *Can. J. Chem.*, 2012, **90**, 666.

18 G. S. Ajmani, D. Goodwin, K. Marsh, D. H. Fairbrother, K. J. Schwab, J. G. Jacangelo and H. Huang, *Water Res.*, 2012, **46**, 5645.

19 C. D. Vecitis, M. H. Schnoor, M. S. Rahaman, J. D. Schiffman and M. Elimelech, *Environ. Sci. Technol.*, 2011, **45**, 3672.

20 G. Gao and C. D. Vecitis, *Environ. Sci. Technol.*, 2011, **45**, 9726.

21 D. Li, J. Tang, X. Zhou, J. Li, X. Sun, J. Shen, L. Wang and W. Han, *Chemosphere*, 2016, **149**, 49.

22 L. Zang, L. Xu, J. He and J. Zhang, *Electrochim. Acta*, 2014, **117**, 192.

23 M. Panizza and G. Cerisola, *Chem. Rev.*, 2009, **109**, 6541.

24 B. Adams, M. Tian and A. Chen, *Electrochim. Acta*, 2009, **54**, 1491.

25 C. J. Miller, H. Yu and T. D. Waite, *Colloids Surf., A*, 2013, **435**, 147.

26 M. F. Hou, L. Liao, W. D. Zhang, X. Y. Tang, H. F. Wan and G. C. Yin, *Chemosphere*, 2011, **83**, 1279.

27 H. Lin, J. Niu, S. Ding and L. Zhang, *Water Res.*, 2012, **46**, 2281.

28 Y. Liu, H. Liu, Z. Zhou, T. Wang, C. N. Ong and C. D. Vecitis, *Environ. Sci. Technol.*, 2015, **49**, 7974.

29 Y. Bessekhouad, R. Brahimi, F. Hamdini and M. Trari, *J. Photochem. Photobiol., A*, 2012, **248**, 15.

30 Z. Sun, H. Zhang, X. Wei, X. Ma and X. Hu, *J. Solid State Electrochem.*, 2015, **19**, 2445.

31 A. M. Zaky and B. P. Chaplin, *Environ. Sci. Technol.*, 2014, **48**, 5857.

32 W. Zhang, H. Kong, H. Lin, H. Lu, W. Huang, J. Yin, Z. Lin and J. Bao, *J. Alloys Compd.*, 2015, **650**, 705.

33 H. Vogt, *Electrochim. Acta*, 1994, **39**, 1981.

34 S. Asim, J. Yin, X. Yue, M. W. Shah, Y. Zhu, Y. Li and C. Wang, *RSC Adv.*, 2015, **5**, 28803.

35 N. D. Mu'Azu, M. H. Almalack and N. Jarrah, *Desalin. Water Treat.*, 2014, **52**, 7293.

36 G. Zhao, X. Cui, M. Liu, P. Li, Y. Zhang and T. Cao, *Environ. Sci. Technol.*, 2009, **43**, 1480.

37 N. G. Tsierkezos and U. Ritter, *J. Chem. Thermodyn.*, 2012, **54**, 35.

38 R. Geng, G. H. Zhao, M. C. Liu and Y. Z. Lei, *Acta Phys.-Chim. Sin.*, 2010, **26**, 1493.

39 J. Yang, J. Wang and J. P. Jia, *Environ. Sci. Technol.*, 2009, **43**, 3796.

40 L. Guo, Y. Jing and B. P. Chaplin, *Environ. Sci. Technol.*, 2016, **50**, 1428.

41 M. C. Santos, Y. A. Elabd, J. Yin, B. P. Chaplin and F. Lei, *AIChE J.*, 2016, **62**, 508.

42 R. Berenguer, J. M. Sieben, C. Quijada and E. Morallón, *Appl. Catal., B*, 2016, **199**, 394.

43 S. Horikoshi, A. Aiko Saitou, H. Hidaka and N. Serpone, *Environ. Sci. Technol.*, 2003, **37**, 5813.

44 Y. Yu, S. Yang, H. He, C. Sun, C. Gu and Y. Ju, *J. Phys. Chem. A*, 2009, **113**, 10024.
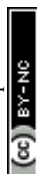
45 T. S. Natarajan, M. Thomas, K. Natarajan, H. C. Bajaj and R. J. Tayade, *Chem. Eng. J.*, 2011, **169**, 126.

46 Z. He, C. Sun, S. G. Yang, Y. C. Ding, H. He and Z. L. Wang, *J. Hazard. Mater.*, 2009, **162**, 1477.

47 D. M. D. Araújo, C. Sáez, C. A. Martínez-Huitle, P. Cañizares and M. A. Rodrigo, *Appl. Catal., B*, 2015, **166**, 454.

48 J. Yang, J. Wang and J. P. Jia, *Environ. Sci. Technol.*, 2009, **43**, 3796.